International Journal of Mass Spectrometry 306 (2011) 150–158

Contents lists available at ScienceDirect

International Journal of Mass Spectrometry

journal homepage: www.elsevier.com/locate/ijms

Implementation of a Penning ionization source on a FTICR instrument with ion funnel optics

Clotilde Le Vot[a], Carlos Afonso[a], Claude Beaugrand[b], Jean-Claude Tabet[a,*]

[a] Equipe de Spectrométrie de masse, Institut Parisien de Chimie Moléculaire, UMR 7201, Université Pierre et Marie Curie-Paris6, 4 place Jussieu, 75252 Paris Cedex 05, France
[b] Alpha-Mos, 20, Avenue Didier Daurat, 31400 Toulouse, France

ARTICLE INFO

Article history:
Received 31 August 2010
Received in revised form
28 September 2010
Accepted 5 October 2010
Available online 14 October 2010

Keywords:
FT-ICR
Penning ionization
Ion funnel
Selectivity
Odd electron ion

ABSTRACT

A Qh-FT-ICR equipped with an electrospray source has been recently coupled, in our laboratory, with a metastable atom bombardment (MAB) source. In this Penning ionization source, the gas phase sample is bombarded with a beam of metastable atoms in vacuum. Compared to EI, the MAB source allows the control of the internal energy and selective ionization by the use of different gases (rare gases and N_2). The FT-ICR provides accurate mass measurements thanks to its ultra-high resolution. After the adaptation of the MAB/EI source and its implementation in the FT-ICR instrument, several optimizations were carried out in order to obtain a detectable signal. The ion beam generated by the dual MAB/EI source was characterized through the study of ion kinetic energy distribution. The FTICR instrument was equipped initially with ESI source and ion funnel optics. The design of the optic lenses and applied potentials used for ions transmission from the homemade EI/MAB dual source to the ESI optics was developed using SIMION simulations. The RF and DC potentials applied to the ion funnels were tuned in order to achieve transmission of low m/z ions with a pressure of 10^{-3} mBar compared to the 1 mBar used in normal ESI operation.

1. Introduction

In the mid 1970s, Fourier Transform Ion Cyclotron Resonance Mass Spectrometry (FT-ICR MS), initiated by Comisarow and Marshall [1], was associated to electron impact ionization and in a lower extent to photoionization. These gas phase ionizations allowed the *in situ* production of odd-electron ions from volatile compounds introduced directly into the ICR cell. This technology has been used to investigate ion-molecule reactions [2–4] and to characterize and identify ions [5]. Its properties allow to achieve unsurpassed resolving power and mass accuracy useful to determine elemental chemical composition. Twenty years later, its improvement was associated to new ionization methods, and especially those which are based on desorption modes. Initially, desorption (*e.g.*, laser desorption (LD) [6] and plasma desorption mass spectrometry (PDMS) [7]) was performed into the ICR cell and more recently, external sources (atmospheric pressure chemical ionization (APCI) [8], atmospheric pressure photoionization (APPI) [9], electrospray [10] desorption electrospray ionization (DESI) [11] and matrix assisted laser desorption ionization (MALDI) [12]) sources have been implemented [13]. The ion beam is transferred through several stages of differential pumping involving either conventional nozzle/skimmer or ion funnel optics [14,15]. These external sources offer several advantages and in particular the decoupling of the ionization and ion analysis step yielding higher flexibility. In order to transfer and activate externally produced ions, hybrid instruments have been introduced. In this case ion selection is often carried out by a quadrupole and a linear ion trap is used for CID and ion accumulation [16,17].

The analysis of complex mixtures such as petrochemical or environmental samples without chromatographic separation can take full advantages of FT-ICR [18]. The ultrahigh resolving power and mass measurement accuracy of this type of instrument allows the simultaneous detection of thousands of species and the attribution, to each ion, of a unique elemental composition. However, due to their complexity resulting from the charged molecular species and their fragment ions, simplifications are required using either computer based data treatment and/or selective ionization [19].

Soft gas phase ionization techniques can be an alternative to EI. They can minimize internal energy which consequently reduce ion fragmentation and simplify the recorded mass spectra. For the analysis of volatile and semi-volatile compounds, the most used techniques are 70 eV electron ionization [20,21], chemical ionization (CI) [22] and field ionization (FI) [23]. Although competitive, each of them has some limitations: an important loss in sensitivity and reproducibility in low-energy EI and FI, and a high background signal in CI. However, Penning ionization as the metastable atom bombardment (MAB) ionization presents many advantages

* Corresponding author. Tel.: +33 1 44 27 32 64; fax: +33 1 44 27 38 43.
E-mail addresses: jean-claude.tabet@upmc.fr, tabet@ccr.jussieu.fr (J.-C. Tabet).

1387-3806/$ – see front matter © 2010 Elsevier B.V. All rights reserved.
doi:10.1016/j.ijms.2010.10.005

[24]. The MAB source uses atoms of rare gases or molecules (N_2) excited to give a flux of metastable neutrals (A^*) able by collision to ionize a target molecule (M) if the process is exothermical (*i.e.*, IE(M) < EE(A), Eq. (1).

$$A^* + M \rightarrow A + M^{+\bullet} + e^- \quad (1)$$

$$E_{int}(M^{+\bullet}) = EE(A) - IE(M) - KE(e^-) \quad (2)$$

where $E_{int}(M^{+\bullet})$: internal energy transferred to the molecular ion; EE(A): excitation energy of metastable atoms or molecules; IE(M): ionization energy of molecule M; $KE(e^-)$: kinetic energy of ejected electron.

The internal energy transferred to the molecular ion (Eq. (2)) depends on the molecule ionization energy and on the excitation energy of the gas metastable state (Table 1S). Thus, by the choice of the gas, the rate constant of fragmentations can be relatively well controlled with a maximum energy $E_{int}^{max}(M^{+\bullet}) = EE(A) - IE(M)$. For instance, with He* and Ne* metastable reagent, the odd-electron molecular ion fragmentation extent is comparable to that provided in EI (70 eV) whereas with Xe* and Kr* the fragmentation pattern is comparable to EI (10 eV) or FI [25]. One particularity of MAB is that the internal energy distribution is relatively narrow compared to EI. The MAB source combines the properties of several ionization methods, without loss of sensitivity in low energy mode contrary to the EI [26]. Moreover, it is possible to selectively ionize only molecules presenting ionization energies lower than the excitation energy of the reactive neutral gas [27]. These advantages (controlled narrow internal energy distribution and selective ionization) are useful for complex mixture analysis. They allow to reduce chemical noise and thus, to facilitate interpretation of mass spectra [25,28].

The MAB ionization has often been compared to electron ionization [29–32]. Using a low excitation energy metastable gas, no reduction of sensitivity is observed with MAB, whereas low energy EI yields a significant loss in sensitivity. These two ionization methods are in fact complementary. In particular EI offer the advantage of its simplicity and the existence of very wide mass spectra library which is a very useful tool for compound identification. Note that competitively, cold EI can be considered as an alternative [33]. Indeed, by the vibrational cooling of neutral analyte from supersonic molecular beam drives down the extent of fragmentations of molecular ions produced under the 70 eV—EI conditions [33].

In this work, we have developed a dual source, which can ionize molecules by electron beam and by metastable atom beam. This dual MAB/EI source was coupled to a commercial hybrid Qh-FT-ICR instrument equipped with ion funnel transfer optics originally designed for ion desolvation and ion transfer. The latter were prepared under high pressure conditions (1 mbar) from solvated ions generated in orthogonal ESI source. This coupling will offer numerous analytical advantages for studying complexes mixtures. The MAB source will lead to a simplification of mass spectra and the potentialities of the FT-ICR mass spectrometer will allow an identification of compounds of interest without ambiguity. For such a purpose, the optimization of the various experimental parameters for ionization and ion transfer will be discussed.

Table 1
Ion beam characterization in term of kinetic energy.

Lens	Mode	$\langle E_{kin} \rangle$[a]	Dispersion[b]
Prefilter of Q1	ESI	4.9	±0.2
	EI	11.9	±0.5
	MAB	12.3	±0.7
Postfilter of Q1	ESI	5.6	±0.5
	EI	12.5	±0.4
	MAB	12.9	±1.0
Entrance lens	ESI	5.3	±0.6
trap/extract of	EI	12.5	±0.3
h2	MAB	13.7	±0.3

[a] Considering symmetric distributions, the average kinetic energy value is estimated as the distribution maximum.
[b] Considering symmetric distributions, the dispersions was determined as the FWHM.

2. Experimental

2.1. FT-ICR instrument

Hybrid Qh-FT-ICR (Bruker Apex-Qe, Bremen, Germany) fitted with an actively shielded 7T super conducting magnet was used (Fig. 1a). This instrument is equipped with an orthogonal Apollo II ESI source controlled by the standalone program Apollo II Control. The Qh-interface and other associated ion transfer optics were controlled by Apex control 2.0 software. This mass spectrometer present ion funnel lenses in the desolvation region. The ion funnel system consists of a series of ring flat electrodes with decreasing internal diameters [15]. The first electrode aperture is large for efficient ion beam acceptance. The co-application of both RF field and DC potential gradient allows to capture, focus, transmit the ion beam and thus to produce an intense and collimated ion beam. Indeed, the oscillating RF fields near the ring electrodes serve to push ions to the weaker electric field region in the central region of the ring electrodes. The low-DC electric field pushed the ions toward the ion funnel exit and buffer gas collisions reduce the ion kinetic energy and damp their motions. Thus, the role of the ion funnel is to reduce both the spatial and kinetic energy distributions of ions after the desolvation step in ESI. Six differential pumping stages maintained by 4 turbo-molecular pumps (TP1–TP4) and 2 mechanical roughing pumps allowed to reach the required ultra high vacuum of $<10^{-10}$ mbar. Ions produced under electrospray conditions were introduced by a dielectric glass capillary into the first vacuum stage maintained at ~4 mbar by a rough pump and accelerated orthogonally into a first electrodynamic ion funnels (IF1). Then, the formed ion beam pass through the second vacuum stage with a second ion funnel (IF2) at ~0.1 mBar and a third vacuum stage with the hexapole (h1) at $\sim 5 \times 10^{-4}$ mBar by TP1. Ions could be trapped between skimmer 2 (Sk2) and the trap/extract electrode before to be transmitted to the fourth vacuum stage of the Qh-interface maintained at $\sim 8 \times 10^{-6}$ mBar by TP2. The latter consists of a mass selective quadrupole filter (Q1), and a second hexapole (h2), which could be used as both an ion storage trap and a collision cell. RF generators provided RF voltages for the ion funnel and hexapole systems at a frequency of ~1 MHz and ~4.5 MHz, respectively. These values strongly influenced the low mass cut-off of the ions. Then, ions are accelerated up to ~3 kV with the first transfer optics and are decelerated and focused through the inhomogeneous fringe field of the superconducting magnet before they reach the analyzer, the *infinity cell*™ [34].

2.2. Source housing

Upstream the FT-ICR instrument, modified source housing from a quadrupole instrument (R10-10, Nermag) was implemented in the axis of the ion funnel optics. The electric connection, the GC interface and direct introduction probe introduction system (with primary pumping) were maintained. However, the flange for calibrant introduction was modified for the installation of the MAB gun. A stainless steel cylinder was built and fixed to the source housing. This cylinder was used for installation of the ion injection optics. The extremity of this tube was designed to be coupled to the FT-ICR source housing. The GC inlet was used for the introduction of volatile sample such as gas or calibrant with glass a reservoir. A needle micro valve controlled the calibrant flow rate. The Nermag

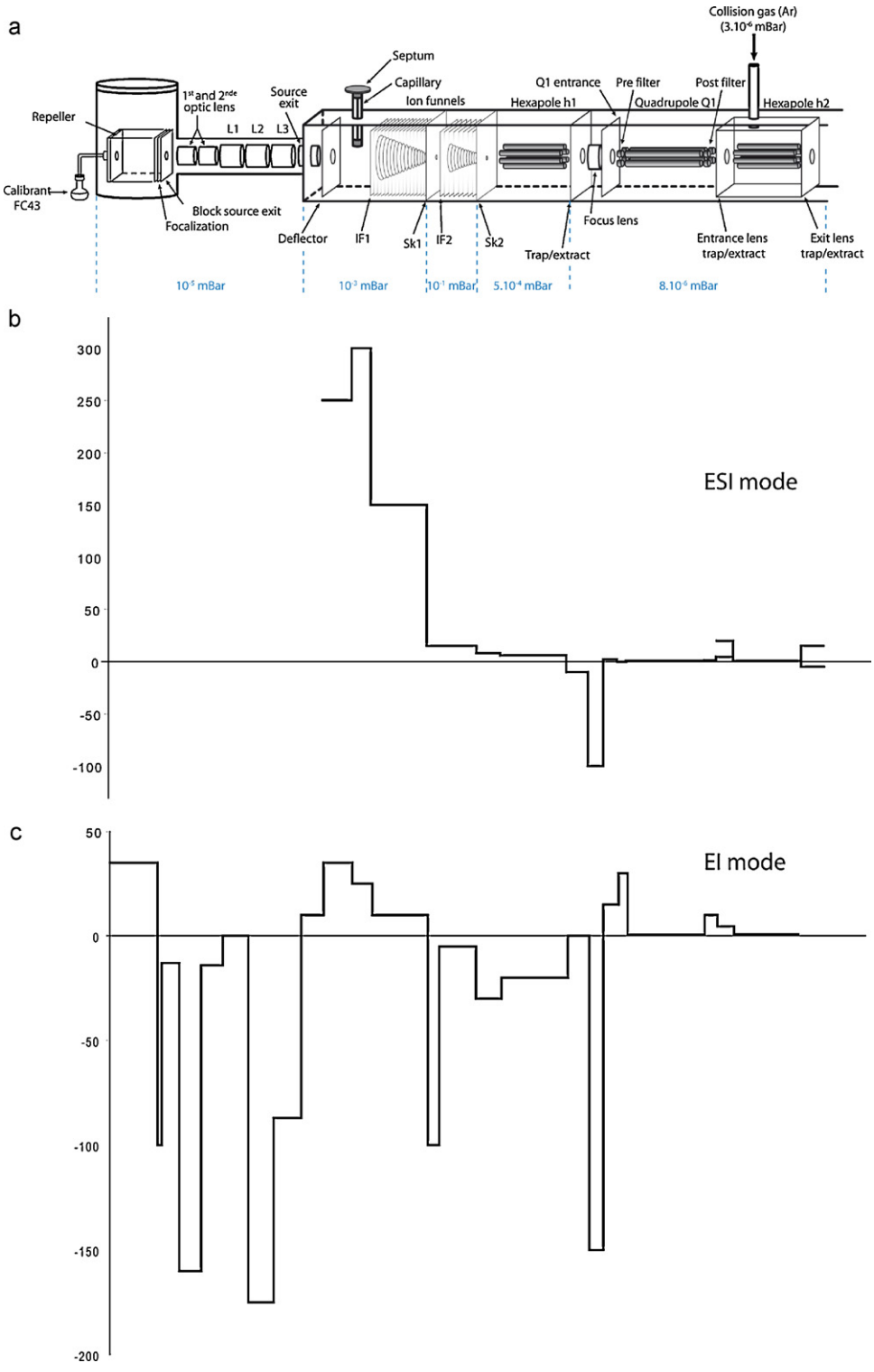

Fig. 1. (a) Scheme of MAB/EI/FT-ICR instrument and voltage diagram for ESI mode (b) and (c) EI/MAB mode.

electronic controller allowed applying potentials to the ion optics and to the dual MAB/EI source. The potentiometer rack designed for controlling the Nermag quadrupole was maintained for controlling the source ion optics.

2.3. Dual EI/MAB source

Inside this source housing, a dual EI/MAB source and the MAB gun were installed and a 250 L/s Varian turbo molecular pump was used to reach a vacuum of $\sim 5 \times 10^{-5}$ mbar. A modified MAB gun from Dephy Technology was used to generate the metastable beam (Fig. 2). This was located close to the source block (0.5 mm) and positioned orthogonally to the axis and to the electron beam. A potential difference of several hundred volts between the cathode and the anode generated a discharge that excited the gas to metastable states in plasma. This plasma is not only composed of metastable atoms, but also electrons, photons and charged species, which can compete with MAB ionization. Consequently, a deflector

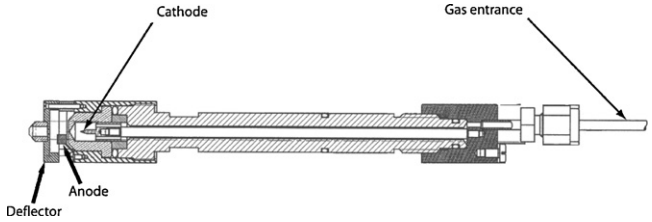

Fig. 2. Scheme of MAB gun (Dephy Technologies).

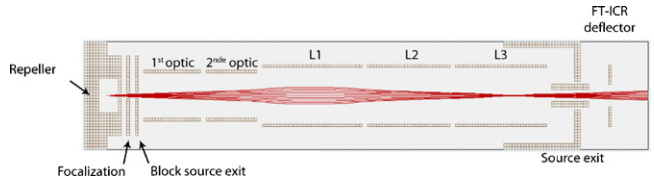

Fig. 3. The injection optic and simulation of ion trajectories using SIMION 7.0.

electrode was used to eliminate the charged species from the source axis. For improving efficiency, this deflector was carefully designed. With adequate polarization, only metastable atoms and photons enter the dual source. The rare gas (or nitrogen) pressure was controlled with a needle valve and measured with a piezoelectric gauge whereas the discharge current and deflector voltage were controlled by a MAB gun power supply (Dephy Technology, Montreal, QC).

The EI/MAB source, based on a Nermag EI source, had three orifices to reach the ionization chamber (Fig. 1S). Originally designed for the calibrant introduction, the first entrance was enlarged for higher acceptance of metastable atom beam produced by the MAB gun. The second entrance, corresponding to GC inlet, was used to introduce calibrant or gas. The third entrance allowed to introduce sample thanks to a direct heated inlet probe. Thus, molecules were ionized by metastable atom beam or by orthogonal electron beam or by both simultaneously. Ion beam was pushed out source by both the repeller and extractor plates to be transferred to the funnel lens entrance thanks to a specially designed ion injection optic using tube lenses. The ion injection optic design was developed using SIMION 7.0 software (SIMION 7.0 beta, D.A. Dahl, Idaho National Engineering Laboratory, Idaho Falls, ID). Note that these ion injection optics permitted a differential pumping between the source region and the funnels inlet. It allows maintaining the low pressure ($\sim 5 \times 10^{-5}$ mbar) in the source housing and a pressure at $\sim 10^{-3}$ mBar at the first funnel. To reach this pressure, it is necessary to plug the ESI source capillary with a GC septum.

2.4. Samples

ESI/FT-ICR instrument was optimized for low mass ions using a solution of the gly_2 dipeptide at a concentration of 30 pmol/μL, prepared in water/methanol (1/1) and HCOOH (0.5%) mixture. For studying ion kinetic energy distributions, a lysine solution was prepared in water/methanol (1/1) and HCOOH (0.5%) mixture with a final concentration of 30 pmol/μL. These solutions were introduced in ESI source with a syringe pump at a flow rate of 160 μL/h. Perfluorotributylamine (FC 43) purchased from Aldrich (Saint Quentin Fallavier, France) was used as calibrant, for optimization of the EI/MAB/FT-ICR instrument and for study of ion kinetic energy distributions. High purity gases (Alphagaz™): xenon, krypton, argon, helium and nitrogen have been purchased from Air Liquide (Nanterre, France).

Anthracene, ethyl-parathion and methyl-parathion/anthracene mixture, purchased from Aldrich (Saint Quentin Fallavier, France), have been use to prepared solutions at a concentration of 400 pmol/μL in MeOH/H_2O (1:1). 2 μL of these solutions were introduced in the quartz tube of the direct introduction probe which was heated from ambient to 200 °C with a gradient of 1 °C/s.

3. Results and discussion

3.1. Optimization of ion beam transfer

The technical coupling between this dual source and the FT-ICR instrument being realized, an optimization of the ion optics parameters has been necessary to transmit low m/z ratio ions efficiently to the ICR cell. Firstly, xenon was used for ion transfer optimization in the EI mode. Secondly FC43 (perfluorotributylamine) was used for calibration and further tuning. Finally, the ion transmission optimization in the MAB mode was easily realized because the conditions in MAB and EI modes were similar.

The potentials applied to the source and the injection optics (focalization up to L3), have been optimized using simulations with SIMION 7.0 software (Fig. 3, Table 2S). In this simulation, the ion kinetic energy was fixed to 35 eV to make sure that ions jump over the pressure barrier between the dual source (at 5×10^{-5} mbar) and ESI source (at 10^{-3} mbar).

To optimize experimentally the low m/z ion transmission in EI mode, xenon gas (introduced by the GC inlet) has been used because it is an atomic gas having a relatively high mass (m/z 131). In order to verify the $Xe^{+\bullet}$ ion beam transmission efficiency along the injection optics, a picoampmeter was connected to the deflector lens (Fig. 1a). By applying the potentials defined during the simulation, no ion current was detected on the deflector lens. This simulation takes no account of the pressure barrier between the source and the desolvatation area. In this case a potential of 50 V on L1 lens was optimal to focalize the ion beam. Experimentally, these potentials had to be decrease to observe a detectable signal on deflector lens. In this way, it was possible to optimize more accurately the potentials applied to the different EI/MAB source (Table 2S). In the end, it was observed that highly negative potentials should be applied on the focalization lens and the first optic to effectively extract ions from the source as well as on the L2 and L3 lenses. The ion beam being accelerated enough to enter the desolvatation area of FT-ICR API source, it was possible to apply a slightly positive potential (10 V) on the source exit lens to focalize the ion beam and thus, to improve the measured ion current.

Since these potentials allowed to reach an intense ion beam on the deflector lens, no ion was detected into ICR cell. Consequently, the transmission parameters of instrument were not adjusted.

3.2. Optimization of FT-ICR parameters (ion funnel lens, hexapole and mass filter potentials) with xenon

The ESI/FT-ICR/MS was usually used to analyze biological molecules, so its parameters are optimized for the detection of relatively higher m/z ratio ions. Consequently, to transfer ion beam with a low m/z ratio range, some FT-ICR parameters must be modified. It was necessary to understand what parameters were important in the transmission of low m/z ratio ions in ESI mode. The observations have been used to optimize the EI mode.

In ESI mode, a solution of gly_2 (Mw 132 u, mass value close to that of $Xe^{+\bullet}$) was used to determinate the optimal conditions (Fig. 1b; Table 3S). The three main parameters influencing the low m/z ion beam transmission efficiency were: (i) the mass fil-

Table 2
Experimental and theoretical m/z ratios of ions present in the MAB (He*) mass spectrum of ethylparathion.

Measured m/z	Theo. m/z	Deviation (ppm)	Elemental composition
291.03242	291.03248	0.2	$C_{10}H_{14}NO_5PS^{+\bullet}$
275.03738	275.03757	0.7	$C_{10}H_{14}NO_4PS^{+\bullet}$
263.00102	263.00118	0.6	$C_8H_{10}NO_5PS^{+\bullet}$
247.97762	247.97771	0.3	$C_7H_7NO_5PS^{+}$
235.97759	235.97771	0.5	$C_6H_7NO_5PS^{+}$
217.96710	217.96714	0.2	$C_6H_5NO_4PS^{+}$
204.97190	204.97189	0.0	$C_6H_6O_4PS^{+}$
185.99504	185.99507	0.2	$C_6H_5NO_4P^{+\bullet}$
171.97423	171.97424	0.0	$C_6H_7NO_5PS^{+\bullet}$
155.00364	155.00355	0.6	$C_6H_5NO_2S^{+\bullet}$
140.00225	140.00217	0.6	$C_6H_5O_2P^{+\bullet}$

ter quadrupole (Q1) settings, (ii) the hexapole RF amplitude and (iii) the "time of flight" delay allowing the ions to fly from the h2 hexapole to the ICR cell. The latter parameter had to be decreased to 6 ms to transfer the gly_2H^+ ions efficiently. Moreover, it has been noticed that the h2 linear ion trap parameters were extremely sensitive; a very weak voltage variation resulted in a complete loss of signal. This work has allowed to optimize the transmission of low m/z ratio ions produced by ESI source operating at a pressure of 1–2 mbar. In the dual source MAB/EI case, the ions are produced in vacuum. Consequently, the transmission conditions optimized in ESI mode may not be directly applicable in EI mode.

In EI mode, the optimal voltages have been determined by measuring the Xe ion current with picoampmeter at each electrode along the ion beam path through the ion funnels and the Q-interface ion optics (Fig. 1c; Table 2S and Table 3S). A significant signal is detected on the deflector lens whereas no signal was obtained at the skimmer 1 lens located just after the first ion funnel (Fig. 1a). This indicates that under the low pressure (*i.e.*, $\sim 10^{-3}$ mbar) conditions, the ions are not able to cross the first ion funnel. Indeed, these lenses were designed to operate under a 1 mbar pressure conditions in ESI mode and seems to limit ion beam transmission at lower pressure. According to the first works of Smith et al. concerning ion funnels [35,36], a pressure decrease in the 1–10 Torr range involved a decrease of the RF amplitude to maintain an efficient ion beam focusing. Consequently, in our work, for pressure even lower ($\sim 10^{-3}$ mBar), it has been necessary to turn off ion funnels RF amplitude, conserving only DC potentials in order to transmit ions efficiently through this optic assimilated to simple lenses. Note that the DC potentials applied on the ion funnel lenses had to be decreased and a high negative potential (−100 V) had to be applied on the skimmer 1 to efficiently extract the ions from the desolvation region.

The optimization of ion transmission through the h1 hexapole and Q1 quadrupole mass filter has been achieved by connecting the picoampmeter on the exit lens of the h2 ion trap (Fig. 1c; Tables 2S and 3S). According to this method, the optimal parameters to transmit the ion beam up the h2 ion trap have been determined.

On normal operating conditions, the ions are accumulated on the h2 ion trap before being transferred to the ICR cell for the excitation/detection step. Nevertheless under such conditions, no ion was observed as shown by the absence of signal from the ICR cell detection plates. For explaining this result, two hypotheses have been considered: (i) the ions trapping in the h2 hexapole did not occur and (ii) the ion current measured by the picoampmeter did not correspond to $Xe^{+\bullet}$ ions. This latter hypothesis is unlikely because the measured ion current depended on the Xe flow introduced in source. However, in order to confirm the presence of $Xe^{+\bullet}$ ions, the EI mass spectrum of its natural isotopic pattern has been recorded as shown in Fig. 4 by manually changing the U/V_{RF} quadrupole filter voltages in isolation mode. Using window of m/z 0.5, the ion current

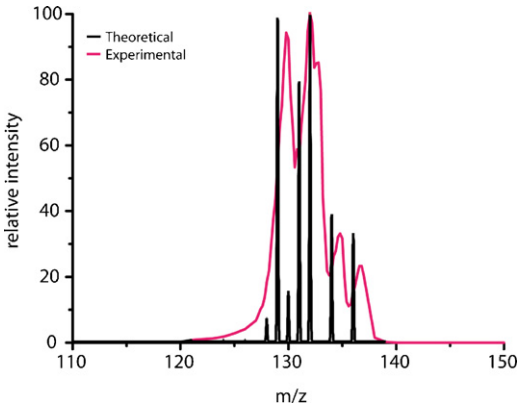

Fig. 4. EI mass spectrum of Xe recorded by manually scanning the quadrupole filter voltages and with ion current detection at the exit trapping/extracting lens.

detection at the h2 exit lens was performed with the picoampmeter.

This experimental measurements showed that the detected ion isotopic distribution corresponded to that of the $Xe^{+\bullet}$ ions in view of the correlation between the theoretical isotopic pattern and the detected ion current. Therefore, it can be concluded that the ions are not efficiently trapped into h2 hexapole. In fact, the potential, applied on the exit trapping/extracting lens, required to stop ion beam was 7 V in the ESI mode and 40 V in EI mode. These observations suggested that kinetic energy of ion beam generated in EI source is too high, and thus the $Xe^{+\bullet}$ ions could not be trapped in the h2 hexapole. In ESI mode, the residual gas (1 mbar) in the ion funnel lenses allows, by collisional relaxation, the kinetic energy cooling of the ions. This phenomenon could not take place in EI mode since the pressure of 10^{-3} mbar in ion funnel lenses was too weak. Consequently, it was necessary to decrease ion kinetic energy to 15 eV by optimizing the different optics located before the h2 hexapole. Indeed, this KE value was sufficiently high to avoid the lost of the ions during their transfer and sufficiently low to trap ions efficiently. The difference of pressure explains mainly the large difference of voltages applied to the ion funnels in ESI and in EI/MAB mode (Fig. 1b and c). For instance, the deflector voltage that is set to around 250 V in ESI is set to around 10 V in the EI/MAB mode. In this way, $Xe^{+\bullet}$ ions could be stored and then, transmitted to the ICR cell to be detected. The optimized potentials for this KE value (15 eV) are reported in Tables 2S and 3S. An optimization of different potentials could be realized with more accurately (Tables 2S and 3S) because the isotopic cluster was visualized directly in the computer. Note that an amplitude at 200 $V_{p,p}$ applied on the h1 hexapole RF allowed a better ion transmission whereas ion funnel RF amplitude should be lower than 10 $V_{p,p}$. Thus, our first Xe mass spectrum was recorded (Fig. 5). Note that the difference of m/z ratio between experimental and theoretical mass spectrum (7 ppm) is due to a bad calibration of the FT-ICR mass spectrometer.

After the tuning with Xe, the FT-ICR calibration in both the EI and MAB modes could be realized by introducing the sample through the GC inlet. The optimum potentials (Tables 2S and 3S) differ from those used for optimization with Xe Indeed, some parameters have been increased such as the RF potential of the Q1 quadrupole filter and h2 hexapole and the time of flight (TOF) to observe the FC 43 fragment ions characterized by m/z values higher than that of the $Xe^{+\bullet}$ ion. The recorded EI and MAB (Ar*) mass spectra (with and without voltage applied on MAB gun deflector) are reported in Fig. 6. The sensitivities obtained in the EI and MAB (Ar*) modes are similar and only relative ion abundances significantly differ. Indeed, MAB (Ar*) ionization is a softer ionization than EI, allowing to reduce dissociation rate constants of fragile fragment ions such as m/z 502. Moreover, if no voltage is applied on MAB gun deflector,

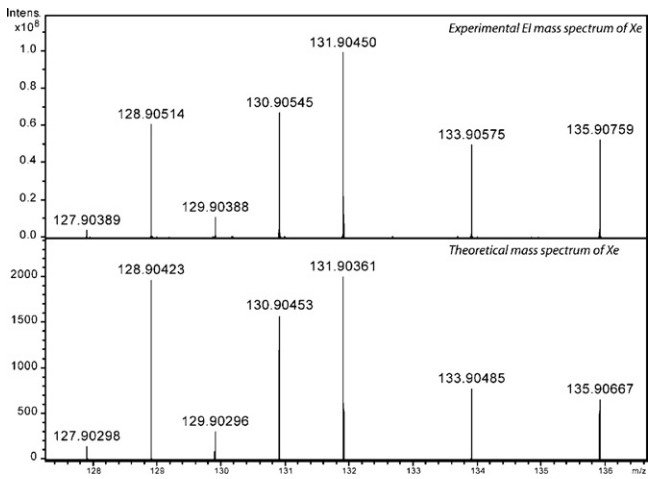

Fig. 5. Experimental and theoretical EI mass spectrum of Xe recorded (average of 50 spectra) without EI calibration.

all species present in plasma (Ar^*, $Ar^{+\bullet}$, e^-) enter in the source and several ionization processes can occur such as Penning and electron ionizations. The recorded mass spectrum (Fig. 6c) is a "mixture" of EI and MAB (Ar^*) mass spectra (Fig. 6a and b).

3.3. Study of kinetic energy distributions of ions produced in the ESI, EI and MAB sources

A kinetic energy distribution of ions was evaluated by the determination of the voltage required to stop the ion beam at different lenses (prefilter and postfilter of quadrupole Q1 and entrance lens trap/extract of hexapole h2). In ESI mode, variation of the MH^+ (m/z 148) abundance as a function of potentials applied on interest lens has been studied whereas in the EI and MAB (Ar^*) modes, the abundance of m/z 464 ions from FC43 was followed. The derivative of the obtained sigmoid yielded the ion kinetic energy distributions. These distributions were characterized by their average kinetic energies $\langle E_{kin} \rangle$ (estimated by their maximum value) and by their distribution dispersions (*i.e.*, Full width at half maximum of the distribution). The measurements are given in Table 1 and the used potentials are presented in Tables 2S and 3S for EI and MAB (Ar^*) modes and in Table 3S for ESI mode.

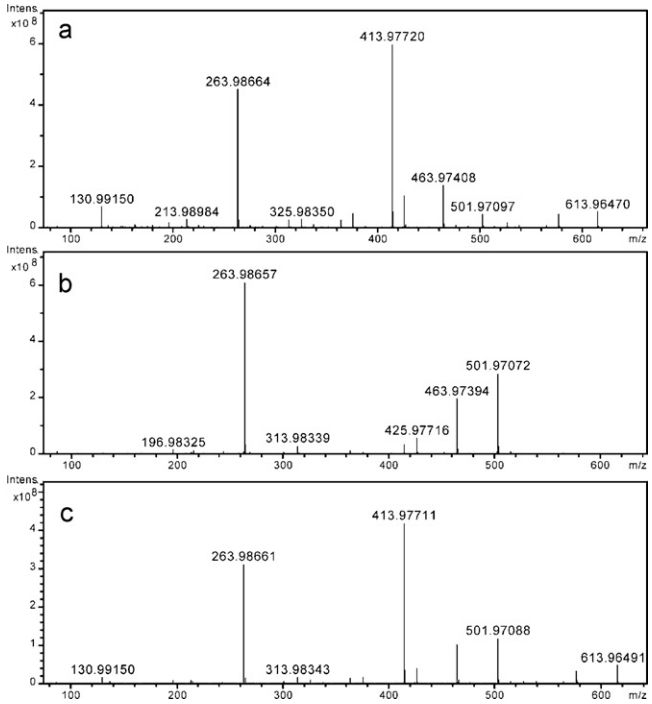

Fig. 6. Mass spectrum of FC 43 recorded with an average of 100 mass spectra in (a) EI mode, (b) MAB(Ar) mode with deflector (−600 V) and (c) MAB mode without deflector. The Argon pressure in MAB gun and discharge voltage was fixed at 10 mBar and 11 V, respectively.

Thus, the ion beam properties in term of $\langle E_{kin} \rangle$ and ion beam dispersion depends on the ionization mode. Ion kinetic energy in the EI and MAB (Ar^*) experiments is two times higher than that obtained in ESI mode. Indeed, in ESI, the presence of relaxation gas at ion funnels allows to slowdown the ions by collisional cooling. In EI and MAB modes, ions did not slow down since the pressure in the desolvation region was weaker and no potential V_{RF} was applied on the ion funnel lenses. The EI and MAB experiments cannot be compared directly because they were not performed in the same conditions (the repeller voltage and ion energy were slightly higher in EI mode). However, despite these highest voltages, the kinetic energy of ions produced in EI mode is slightly lower (0.4 eV) than that of ions produced mode MAB (Ar^*). A possible explanation is that the electron beam attracts slightly ions causing a decrease in the ion kinetic energy at the source exit. In addition, it can be observed that the ion kinetic energy in EI and MAB modes increases along their transfer.

3.4. Application of homemade MAB/FT-ICR instrument

The MAB source allows controlling the fragmentation extent of $M^{+\bullet}$ molecular ion that depends on the internal energy transferred to this ion (Eq. (2)). During Penning ionization (Eq. (1)), the kinetic energy distribution of ejected electron extending from 0 eV to a maximum [EE(A*) − EI(M)] eV the distribution of the internal energy transferred to molecular ion $M^{+\bullet}$ can take any values from [EE(A*) − EI(M)] eV to 0 eV, Eqs. (3) and (4). Consequently, by the choice of the metastable gas, it is possible to know the maximum internal energy of the molecular ion and, thus, to control its fragmentation extent.

$$E_{int}^{max}(M^{+\bullet}) = EE(A^*) - IE(M) \quad \text{when} \quad E_k(e^-) \to 0 \tag{3}$$

$$E_{int}^{min}(M^{+\bullet}) \to 0 \quad \text{when} \quad E_k(e^-) \to EE(A^*) - IE(M) \tag{4}$$

In order to validate the potentiality of the MAB/FTICR to control fragmentations, mass spectra of anthracene (Mw = 178.07770 u, $C_{14}H_{10}$) have been recorded using both the 70 eV EI and MAB modes (with different metastable reagent gases, Fig. 7). The ionization energy of anthracene (IE = 7.44 eV [37]) is lower than the excitation energies of all the used metastable species. Thus, anthracene molecule can be ionized independently to the chosen reagent metastable gases. If the energy excess is sufficient, fragment ions can be produced and in particular losses of H_2 and C_2H_2. The excitation energy of He* [*i.e.*, EE(He*) = 19.82 eV] being relatively high, the distribution of internal energy transferred to anthracene is large (from 0 eV to 12.38 eV). This internal energy excess is sufficient to generate extensive fragmentations from ionized anthracene. Consequently, He reagent gas allow to obtain information on the structure of studied compounds. The MAB (He*) mass spectrum of anthracene is similar to that of EI mass spectrum: the same fragment ions are present but are formed with higher relative abundance in MAB (He*) mode. Xe* metastable gas is characterized by a very weak excitation energy (EE(Xe*) = 8.32 eV) but slightly higher than the ionization energy of anthracene. Under these conditions, the anthracene molecular ion is characterized by an internal energy close to the minimum of energy which leads to almost no fragmentation. In this way, only the molecular ion is displayed in the Xe* mass spectra, facilitating the

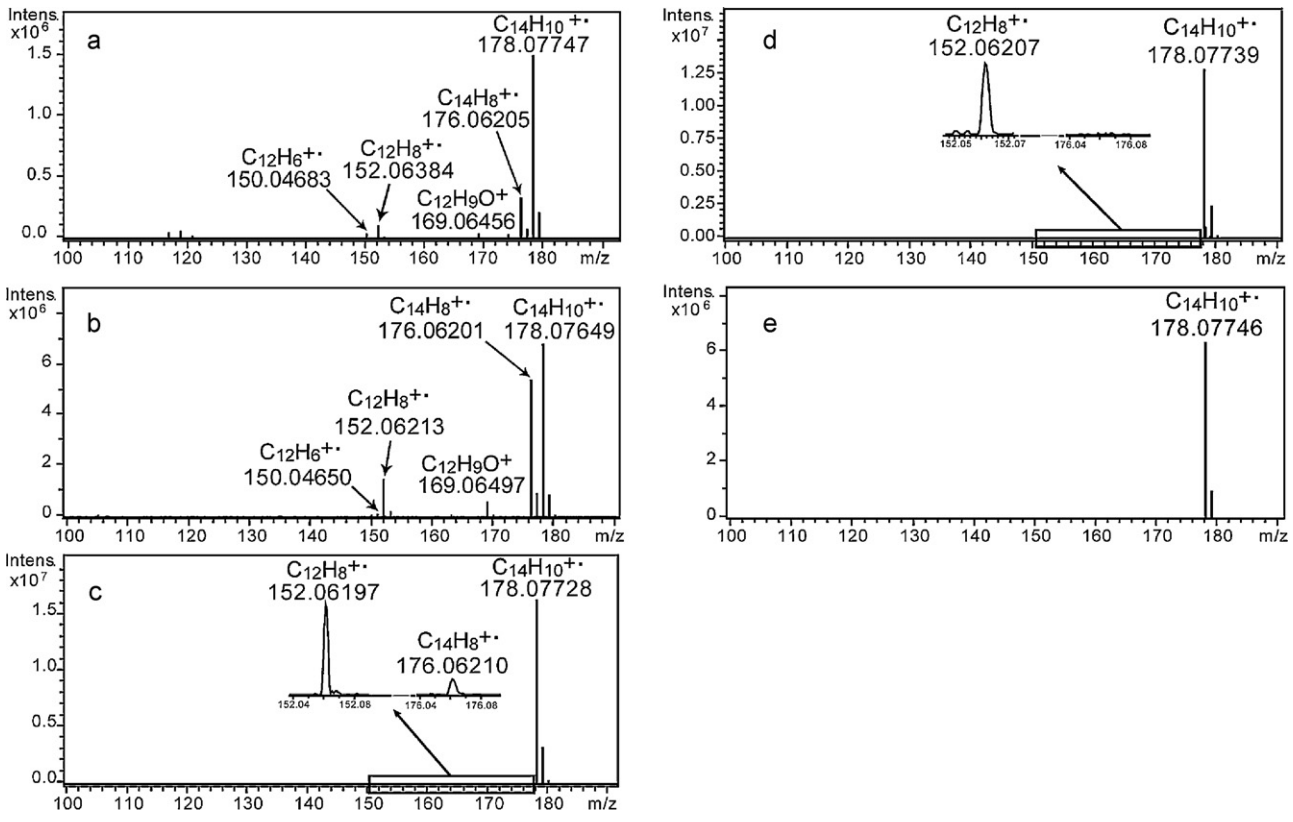

Fig. 7. Mass spectra of anthracene by gas phase ionization modes: (a) EI (70 eV), and MAB using as reagent metastable gases: (b) helium, He*, (c) argon, Ar*, (d) krypton, Kr* and (e) xenon, Xe*.

detection and identification of molecules present in complex mixtures. From these experimental results, it appears that MAB is as sensitive as EI in view of the observed ion abundances (Fig. 7a and b).

The situation is similar for other classes of compounds (*e.g.*, pesticides) which correspond to molecules more fragile than aromatic systems. Fig. 8 presents the mass spectra recorded for ethyl-parathion (Mw 291 u) under EI and MAB conditions. It can be

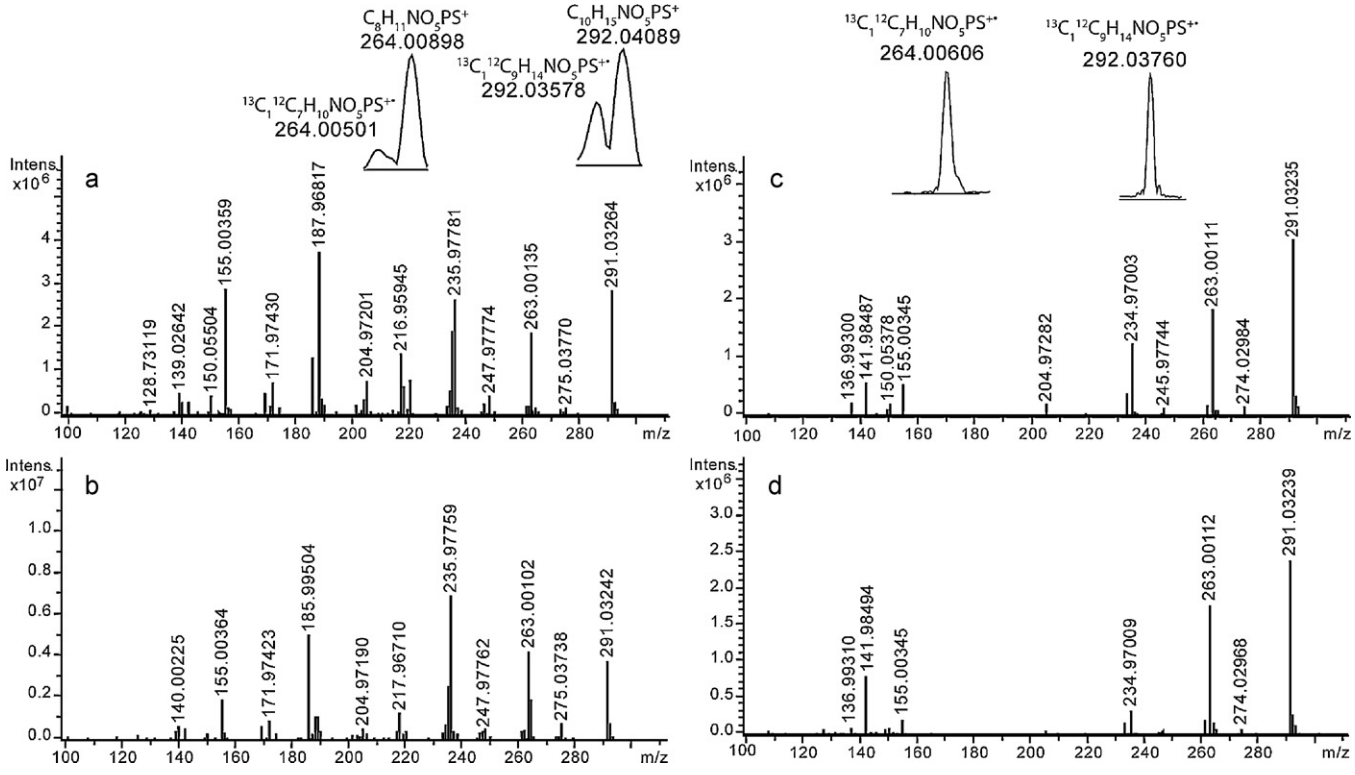

Fig. 8. Mass spectra of ethyl-parathion by (a) EI (70 eV), (b) MAB (He*), (c) MAB (Ar*) and (d) MAB (Kr*). Insets are zooms of *m/z* 264 and 292 ions.

observed that the use of the He* metastable reagent to ionize ethyl-parathion yields extended fragmentations, which are comparable to EI mode. However, in this case, Penning ionization seems to transfer slightly less vibrational/electronical energy since the consecutive dissociation are produced in a lower abundance. The Ar* and Kr* metastable reagents lead to limited fragmentations (Fig. 8c and d). The main fragment ions are the *m*/*z* 263 and *m*/*z* 235 ions produced by consecutive losses of $CH_2{=}CH_2$ from the molecular ion. It should be noted that in Fig. 8a and b, an ion at *m*/*z* 236 is observed. It is unlikely that this ion is directly produced from the *m*/*z* 291 molecular ion. However, careful scrutiny of the mass spectra allowed us to determine that this *m*/*z* ion is only observed when the *m*/*z* 292 ion and *m*/*z* 264 ions are present (insets of Fig. 8a and c). Consequently, the *m*/*z* 292 ion is most likely produced through self-chemical ionization [22,38]. Indeed, low *m*/*z* fragment ions present in the ionization chamber are able to ionize the M molecule through proton transfer, yielding the protonated molecule MH^+. In this case, the *m*/*z* 264 and *m*/*z* 236 ions are produced by losses of ethene from the MH^+ ion. This interpretation is consistent with the fact that these species are not detected in Fig. 8c and d presenting low fragmentation extent. This MH^+ ion formation can create problem for mass spectra identification using a library search. It should be noted that no signal was detected using Xe* as metastable reagent.

The MAB source is also able to perform selective ionization by eliminating the presence of chemical background in the mass spectra. For illustrating this potentiality, a mixture of methyl-parathion/anthracene was analyzed with the He* and Xe* metastable reagent. The use of He* gas allows to ionize all molecules present in mixture whereas the use of Xe* gas allows to ionize only the compound having ionization energy lower than the excitation energy of Xe, *i.e.*, anthracene. It is possible to estimate the unknown ionization energy of methyl-parathion from experimental results as this compound is ionized by Kr but not by Xe. Consequently, we can conclude that the ionization energy of methyl-parathion is between the Xe excitation energy and the Kr excitation energy, *i.e.*, between 8.32 eV and 9.92 eV.

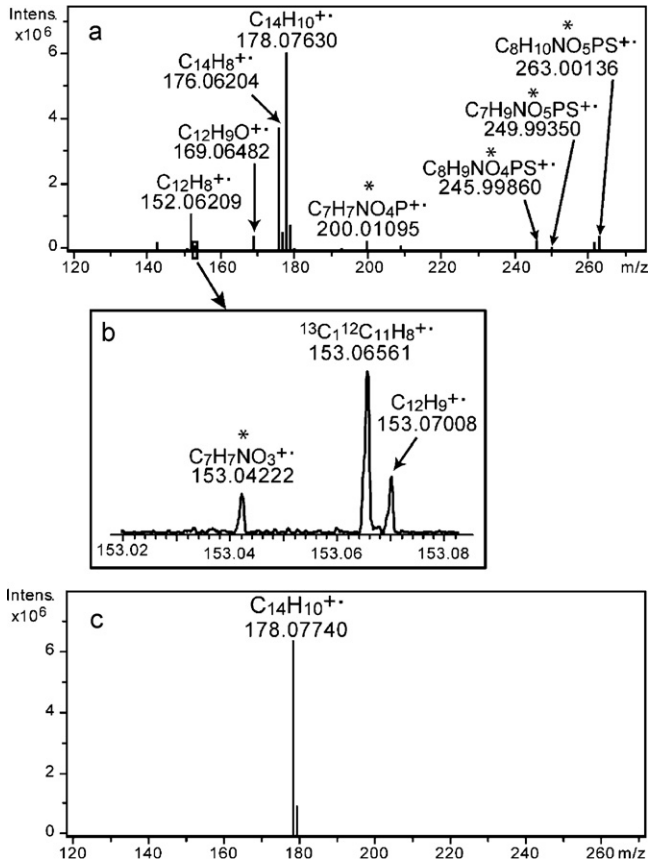

Fig. 9. Mass spectra of a mixture of methyl-parathion/anthracene by MAB (He*) (a) with a zoom (b) and MAB (Xe*) (c). *The ionized ions from methyl-parathion are marked by asterisks.

Furthermore, with the ultra-high resolving power of the FT-ICR, the identification of isobaric ions becomes possible unambiguously by performing accurate mass measurements (Fig. 9). Fig. 9b shows the possibility to detect, at the same nominal *m*/*z* ratio, the $C_7H_7NO_4^{+\bullet}$ ion (fragment ion of methyl-parathion), the $C_{12}H_9^{+\bullet}$ ion (fragment ion of anthracene) and the $^{13}C_1{}^{12}C_{11}H_8^{+\bullet}$ natural isotopic ion of the $C_{12}H_8^{+\bullet}$ ion. Moreover, the accurate mass measurements with deviations lower than 1 ppm allow obtaining the unique elemental composition of the different ions (Table 2). This advantage is essential in the analysis of complex mixtures for rejecting false positive.

4. Conclusion

In this work, we have realized the coupling of a Penning ionization source with a FTICR instrument equipped initially with ESI source and ion funnel optics. The design of the optic lenses and applied potentials used for ions transmission from the home-made EI/MAB dual source to the ESI optics was developed using SIMION simulations. The RF and DC potentials applied to the ion funnels were tuned in order to achieve transmission of low *m*/*z* ions with a pressure of 10^{-3} mBar compared to the 1 mBar used in normal ESI operation. The optimal voltages are very different from the standard voltages used in ESI and were determined by measuring ion current at each electrodes along the different ion optics. After leaving the ion funnels, the ion beam was transmitted using the hexapole and a quadrupole of the commercial Qh-FTICR instrument and is trapped in the linear ion trap before being transmitted to the ICR cell. This storage step was crucial and required an accurate tuning of the ion kinetic energy to avoid the loss of the transferred ions. The design of the system was presented together with description of the used parameters. In addition, determination of ion kinetic energy dispersion was carried out in both the EI and Penning modes.

The MAB/FT-ICR instrument presents numerous advantages for the analysis of complex mixtures, without preliminary chromatographic separation. Indeed, the possibility of using different metastable gases having a low excitation energy (Kr and Xe), allows to limit fragmentations and to hinder the interfering compounds by selective ionization. Thus, the identification of the various compounds present in the mixture is simplified. Moreover, the ultra-high resolution of the FT-ICR instrument allows to measure accurate *m*/*z* ratios (deviations <1 ppm) of ions and to distinguish the isobaric ions by their elemental composition. In the future, the potentiality of MAB/FT-ICR to analyze complex mixtures will be verified.

Acknowledgements

DGA, NRBC Program of CEA, University Pierre and Marie Curie and CNRS are gratefully acknowledge for financial support. Dr. Xavier Machuron is gratefully acknowledged for helpful discussion.

Appendix A. Supplementary data

Supplementary data associated with this article can be found, in the online version, at doi:10.1016/j.ijms.2010.10.005.

References

[1] M.B. Comisarow, A.G. Marshall, Chem. Phys. Lett. 25 (1974) 282–283.
[2] K. Eller, H. Schwarz, Chem. Rev. 91 (1991) 1121–1177.

[3] B.S. Freiser, Fourier transform mass spectrometry, in: J.M. Farrar, W.H. Saunders Jr. (Eds.), Techniques for the Study of Ion Molecule Reactions, vol. 20, Wiley, New York, 1988, pp. 61–118.
[4] N.M.M. Nibbering, Gas-phase ion/molecule reactions as studied by Fourier transform ion cyclotron resonance, Acc. Chem. Res. 23 (1990) 279–285.
[5] B. Asamoto, R.C. Dunbar, Analytical Applications of Fourier Transform Ion Cyclotron Resonance Mass Spectrometry, New York (1991) p. 306.
[6] C.L. Wilkins, D.A. Weil, C.L.C. Yang, C.F. Ijames, Anal. Chem. 57 (1985) 520–524.
[7] (a) J.C. Tabet, J. Rapin, M. Poretti, T. Gaumann, Chimia 40 (1986) 169–171;
(b) F.W. McLafferty, I.J. Amster, J.J.P. Furlong, J.A. Loo, B. H. Wang, E.R. Williams, Tandem Fourier Transform Mass Spectrometry of Large Molecules, Fourier Transform Mass Spectrometry (1987) Chapter 7, pp. 116–126.
[8] Y.H. Kim, S. Kim, J. Am. Soc. Mass Spectrom. 21 (2010) 386–392.
[9] (a) M.J. Greig, B. Bolanos, T. Quenzer, J.M.R. Bylund, Rapid Commun. Mass Spectrom. 17 (2003) 2763–2768;
(b) J.M. Purcell, C.L. Hendrickson, R.P. Rodgers, A.G. Marshall, Anal. Chem. 78 (2006) 5906–5912.
[10] K.D. Henry, E.R. Williams, B.H. Wang, F.W. McLafferty, J. Shabanowitz, D.F. Hunt, Proc. Natl. Acad. Sci. U.S.A. 86 (1989) 9075–9078.
[11] M.S. Bereman, L. Nyadong, F.M. Fernandez, D.C. Muddiman, Rapid Commun. Mass Spectrom. 20 (2006) 3409–3411.
[12] J.A. Castro, C. Koster, C. Wilkins, Rapid Commun. Mass Spectrom. 6 (1992) 239–241.
[13] A.G. Marshall, C.L. Hendrickson, G.S. Jackson, Mass Spectrom. Rev. 17 (1998) 1–35.
[14] P. Kofel, T.B. McMahon, Int. J. Mass Spectrom. Ion Proc. 98 (1990) 1–24.
[15] S.A. Shaffer, K. Tang, G.A. Anderson, D.C. Prior, H.R. Udseth, R.D. Smith, Rapid Commun. Mass Spectrom. 11 (1997) 1813–1817.
[16] S.M. Patrie, J.P. Charlebois, D. Whipple, N.L. Kelleher, C.L. Hendrickson, J.P. Quinn, A.G. Marshall, B. Mukhopadhyay, J. Am. Soc. Mass Spectrom. 15 (2004) 1099–1108.
[17] P.B. O'Connor, J.L. Pittman, B.A. Thomson, B.A. Budnik, J.C. Cournoyer, J. Jebanathirajah, C. Lin, S. Moyer, C. Zhao, Rapid Commun. Mass Spectrom. 20 (2006) 259–266.
[18] A.G. Marshall, Int. J. Mass Spectrom. 200 (2000) 331–356.
[19] C.A. Hughey, R.P. Rodgers, A.G. Marshall, Anal. Chem. 74 (2002) 4145–4149.
[20] S. Guan, A.G. Marshall, S.E. Scheppele, Anal. Chem. 68 (1996) 46–71.
[21] R.P. Rodgers, F.M. White, D.G. McIntosh, A.G. Marshalla, Rev. Sci. Instrum. 69 (1998) 2278–2284.
[22] S. Ghaderi, P.S. Kulkarnl, E.B. Ledford Jr., C.L. Wilkins, M.L. Gross, Anal. Chem. 53 (1981) 428–437.
[23] T.M. Schaub, C.L. Hendrickson, K. Qian, J.P. Quinn, A.G. Marshall, Anal. Chem. 75 (2003) 2172–2176.
[24] F.M. Penning, Naturwissenschaften 15 (1927) 818.
[25] S. Letarte, D. Morency, J. Wilkes, M.J. Bertrand, J. Anal. Appl. Pyrol. 71 (2004) 13–25.
[26] H.E. Lumpkin, T. Aczel, Anal. Chem. 36 (1964) 181–184.
[27] D. Faubert, G.J.C. Paul, J. Giroux, M.J. Bertrand, Int. J. Mass Spectrom. Ion Proc. 124 (1993) 69–77.
[28] S. Moore, Chemosphere 49 (2002) 121–125.
[29] M. Boutin, J. Lesage, C. Ostiguy, M.J. Bertrand, J. Anal. Appl. Pyrol. 70 (2003) 505–517.
[30] M.G. Ikonomou, S. Rayne, Anal. Chem. 74 (2002) 5263–5272.
[31] C.K. Fagerquist, M.K. Hellerstein, D. Faubert, M.J. Bertrand, J. Am. Soc. Mass Spectrom. 12 (2001) 754–761.
[32] M. Mousselmal, D. Faubert, M.J. Evans, M.J. Bertrand, Proc. 44th ASMS Conf. Mass Spectrom. (1996).
[33] A. Amirav, A. Gordin, M. Poliak, T. Alon, A.B. Fialkov, J. Mass. Spectrom. 43 (2008) 141–163.
[34] P. Caravatti, M. Allemann, Org. Mass Spectrom. 26 (1991) 514–518.
[35] S.A. Shaffer, D.C. Prior, G.A. Anderson, H.R. Udseth, R.D. Smith, Anal. Chem. 70 (1998) 4111–4119.
[36] S.A. Shaffer, A. Tolmachev, C. Prior David, G.A. Anderson, H.R. Udseth, R.D. Smith, Anal. Chem. 71 (1999) 2957–2964.
[37] J.W. Hager, S.C. Wallace, Anal. Chem. 60 (1988) 5–10.
[38] N. Méchin, J. Plomley, R.E. March, T. Blasco, J.-C. Tabet, Rapid Commun. Mass Spectrom. 9 (2005) 5–8.